




Article

The Amplification and Polarization Control of Transmitted Radiation by a Graphene-Containing Photonic Cell

Svetlana V. Eliseeva ^{*} , Pavel A. Itrin  and Dmitriy I. Sementsov Department of High Technology Physics and Engineering, **Ulyanovsk State University**, Lev Tolstoy 42, 432700 Ulyanovsk, Russia

* Correspondence: eliseeva-sv@yandex.ru

Abstract: The transformation of the transmission spectra of linearly polarized radiation passing through a symmetric photonic cell is studied based on numerical analysis. The cell consists of two layers of magnetic semiconductor with a graphene monolayer on each and a central dielectric layer located between the graphene monolayers. It is possible to achieve amplification in the near terahertz range in graphene layers due to charge carrier drift. Control of transmission spectra and polarization of transmitted radiation can be achieved by changing the Fermi energy of graphene layers, by changing the external magnetic field, and by changing the thickness of the dielectric layer and the orientation of the incident radiation polarization plane.

Keywords: symmetric photonic cell; one-dimensional photonic-crystal; transmission spectra; microcavities

1. Introduction

Planar photonic crystal structures with various combinations of their constituent layers have attracted close attention of researchers due to their capabilities for effective control of optical radiation [1–5]. Control of reflection and transmission spectra for such structures, as a rule, is achieved by including layers in their composition, the material parameters of which depend on easily variable external factors (electric and magnetic fields, angle of incidence and polarization of incident radiation) [6–10]. Photonic crystal structures are used to create a wide class of radiation control devices (filters, switches, modulators), performing the function of filtering and amplifying various types of propagating waves [11–14].

The presence of the photonic band gaps in the photon spectrum is characteristic of one-dimensional layered periodic structures. Violation of periodicity in the structure leads to the appearance of a narrow transmission band in the photonic band gap. Microcavities are similar structures, the formation of which requires two Bragg mirrors (BMs) with a change in the order of layers in one of them. The working cavity (the area between the mirrors), as a rule, is filled with an active medium. Standing waves are established in the working cavity, and transmission resonances (defect modes) arise in the photonic band gap if the distance between the BMs is a multiple of half the propagating radiation wavelength.

The contrast of the photonic band gap and the defect mode in the spectrum significantly depends on the number of periods in the BMs; with their increase, the contrast increases. In this regard, it is of interest to consider the properties of a photonic cell (PC) with a minimum number of periods in BMs, which can also be considered as a microcavity with fairly effective control of the radiation passing through it (or reflected). Graphene and various planar structures based on it can be considered the most promising photonic materials. Graphene is a 2D structure and has a number of unique properties: zero band gap, high electron mobility, high optical transparency [15–19]. Graphene may have the properties of an amplifying medium when excited and creates an inversion in its energy structure [20–22]. The active state of graphene can be obtained through the drift of charge carriers as a result of current pumping. Doped and inverted graphene is discussed in



Citation: Eliseeva, S.V.; Itrin, P.A.; Sementsov, D.I. The Amplification and Polarization Control of Transmitted Radiation by a Graphene-Containing Photonic Cell. *Photonics* **2023**, *10*, 1318. <https://doi.org/10.3390/photonics10121318>

Received: 30 October 2023

Revised: 26 November 2023

Accepted: 28 November 2023

Published: 29 November 2023



Copyright: © 2023 by the authors. Licensee MDPI, Basel, Switzerland. This article is an open access article distributed under the terms and conditions of the Creative Commons Attribution (CC BY) license (<https://creativecommons.org/licenses/by/4.0/>).

paper [21,22], decorated graphene is discussed in paper [23]. In recent years, structures called “photonic graphene” have been of great interest. These are two-dimensional meta-surfaces made of nano- or microparticles located in space according to a certain law at distances shorter than the wavelength of propagating radiation. An important property of such gratings is tunability under external influence, the role of which can be played by the intensity of the light wave, polarization, magnetic field, temperature [24,25].

In this work, the photonic properties of one of the possible symmetrical graphene-containing photonic cells are studied based on a numerical analysis of the general relationships for the transmission (reflection) coefficients and polarization characteristics of a planar layered magnetically active structure, in which the active state of graphene is achieved due to the drift of charge carriers as a result of current pumping. It has been shown that it is possible to effectively control the transmission and reflection spectra, as well as the polarization of transmitted radiation, by changing the Fermi energy of graphene, by changing the external magnetic field, by changing the thickness of the dielectric (the gap between the graphene layers), and also by changing the orientation of the polarization plane incident radiation.

2. Geometry and Material Parameters of a Photonic Cell

From the many possible types of PCs, we study a cell (*ms/g/d/g/ms*), consisting of two layers of a magnetic semiconductor (*ms*), two graphene monolayers (*g*), separated by a dielectric layer (*d*), the thickness of which can be changed during the experiment (such a dielectric can be an air gap). A PC is shown schematically in Figure 1.

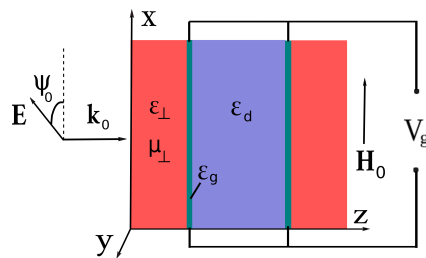


Figure 1. Structure of a photonic cell.

As a magnetically active material, we have chosen a well-studied magnetic semiconductor *CdCr₂Se₄*, which combines the properties of a semiconductor (sufficiently high conductivity, can be *p*- and *n*-type depending on the production method) and a magnetic (sufficiently high magnetization) [26]. This material is characterized by cyclotron and ferromagnetic resonances with a narrow width of the resonance curve, which significantly expands the possibilities of its practical application [27].

The permittivities and permeabilities of such a material are tensor quantities:

$$\hat{\epsilon} = \begin{pmatrix} \epsilon & 0 & 0 \\ 0 & \epsilon & i\epsilon_a \\ 0 & -i\epsilon_a & \epsilon \end{pmatrix}, \quad \hat{\mu} = \begin{pmatrix} \mu & 0 & 0 \\ 0 & \mu & i\mu_a \\ 0 & -i\mu_a & \mu \end{pmatrix}. \tag{1}$$

The components of the dielectric permittivities tensor are given by the relations [28]:

$$\epsilon = \epsilon_l \left(1 + \frac{\omega_p^2 \omega_v}{\omega(\omega_v^2 - \omega_c^2)} \right), \quad \epsilon_{\parallel} = \epsilon_l \left(1 - \frac{\omega_p^2}{\omega \omega_v} \right), \quad \epsilon_a = \frac{\epsilon_l \omega_p^2 \omega_c}{\omega(\omega_v^2 - \omega_c^2)}, \tag{2}$$

where plasma and cyclotron frequencies are introduced $\omega_p = \sqrt{4\pi e^2 n_0 / m^* \epsilon_l}$ and $\omega_c = eH_0 / m^* c$. For numerical modeling, we will use the parameters of the above *p*-type magnetic semiconductor: $\epsilon_l \simeq 17.8$ is the lattice part of the permittivity, n_0 and m^* is the concentration of carriers $n_0 = 6 \cdot 10^{14} \text{ cm}^{-3}$, their effective mass $m^* = 0.1 m_e$, $\omega_v = \omega + i\nu$, collision frequency $\nu = 10^{11} \text{ s}^{-1}$ [26,28]. The effective permittivity is $\epsilon_{\perp} = \epsilon - \epsilon_a^2 / \epsilon$ taking

into account the transverse orientation of the external magnetic field with respect to the wave vector ($\mathbf{k} \perp \mathbf{H}_0$). Note the resonant nature of the dependencies $\varepsilon_{\perp}(\omega, H_0)$. For each value H_0 , in a narrow region near the frequency $\omega_{res} \simeq \sqrt{\omega_p^2 + \omega_c^2}$ there is a sharp increase in the imaginary part of the effective permittivity, which should lead to sharp dips in the transmission spectrum at these frequencies.

The non-zero components of the permeability tensor $\mu_{yy} = \mu_{zz} = \mu$, μ_{xx} , $\mu_{yz} = -\mu_{zy} = i\mu_a$ have the form [29]:

$$\mu = 1 + \frac{\omega_M(\omega_H + i\Delta\omega)}{\omega_H^2 - \omega^2 + 2i\omega_H\Delta\omega'}, \quad \mu_a = \frac{\omega_M\omega}{\omega_H^2 - \omega^2 + 2i\omega_H\Delta\omega'}, \quad \mu_{xx} = 1, \quad (3)$$

where $\omega_M = 4\pi\gamma M_0$, $M_0 = 220$ G is the saturation magnetization, $\omega_H = \gamma H_0$, $\Delta\omega = \gamma\Delta H$ is the magnetic resonance linewidth, γ is the gyromagnetic ratio. Effective permeability for the considered geometry $\mu_{\perp} = \mu - \mu_a^2/\mu$.

Figure 2 shows the frequency dependences of the imaginary part of the effective permittivity and permeability obtained at $H_0 = (0, 5, 10, 15)$ kOe (black, red, blue, green curves), which correspond to absorption lines at cyclotron and ferromagnetic resonances. The maxima of these dependencies lie in the low-frequency terahertz region for permittivities and in the microwave region for permeability. The maxima of these dependencies correspond to cyclotron and magnetic resonances. It is possible to control the material parameters of an effective medium using a magnetic field; this follows from the given dependencies. In this case, an increase in the external magnetic field shifts the resonance curves to higher frequencies.

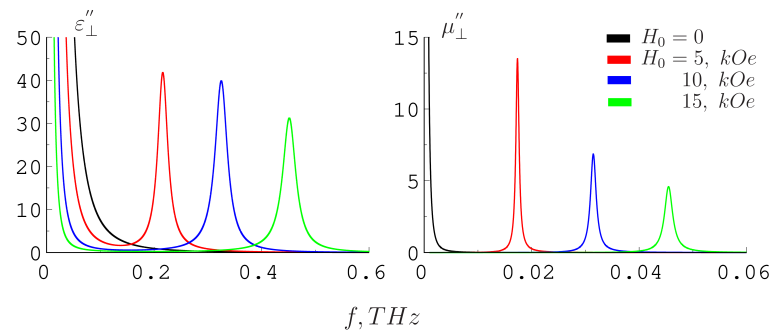


Figure 2. Frequency dependence of the imaginary part of the effective permittivity and permeability at $H_0 = (0, 5, 10, 15)$ kOe (black, red, blue, green curves).

The terahertz response of a graphene monolayer carrying a direct current for frequencies below the electron-electron collision frequency is determined by its surface conductivity σ_g . Due to the strong electron-electron interaction in graphene, it is correct to use the hydrodynamic approach at the indicated frequencies. The expression for the surface conductivity of graphene, valid for the low frequency region ($f < 5$) THz and obtained in the hydrodynamic approximation [30–33], taking into account the normal incidence of the wave on the layer, has the form

$$\frac{\sigma_g}{\sigma_0} = \frac{4E_F\omega [3\gamma\beta + 2i\omega(1 - \beta)]}{\pi\hbar\sqrt{1 - \beta}\omega^2(i - \gamma/\omega) [3\gamma\beta + i\omega(\beta - 2)]}. \quad (4)$$

Here the surface conductivity of graphene is introduced $\sigma_0 = e^2/4\hbar$, E_F is the Fermi energy in the absence of carrier drift, $\beta = (u/V_F)^2$ is a parameter, V_F and u are the Fermi speed and the drift speed, which is determined by the magnitude of the applied static electric field (V_g is the potential difference between the graphene layers). The real part of the graphene conductivity becomes negative at drift speeds greater than the phase speed of the electromagnetic wave, and due to the Vavilov-Cherenkov effect in the terahertz range, amplification is achieved [31,32].

Figure 3 shows the dependence of the conductivity real part of graphene on the frequency (a), obtained on the basis of Equation (4) for the values $u = 0.75 V_F$, $E_F = (50, 100, 200)$ meV (red, green, blue curves) and $V_F = 10^6$ m/s, $\tau = 0.2$ ps. Figure 3b,c shows the conductivity maps of the dependences $\sigma'_g(\beta, f)$ and $\sigma'_g(E_F, f)$, which make it possible to determine the conductivity value for any values of the specified parameters. Dotted lines separate positive and negative values σ'_g . Thus, the real part of the conductivity $Re\sigma_g$ takes negative values and graphene becomes an amplifying medium in the frequency range $f < 1$ THz at non-zero Fermi energy values. The combination of the frequency ranges of graphene amplification and the resonances of the material parameters of a magnetic semiconductor indicates that using an external magnetic field it will be possible to control the optical characteristics of a photonic cell.

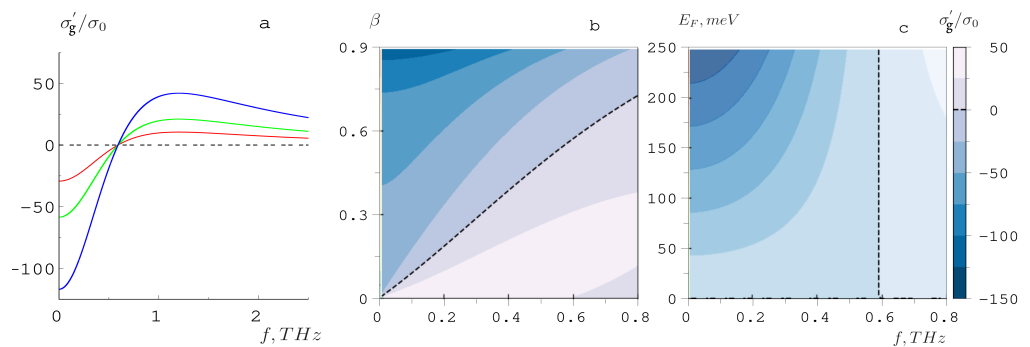


Figure 3. (a) Frequency dependence of the graphene conductivity real part at $E_F = (50, 100, 200)$ meV (red, green, blue curves), (b) the graphene conductivity real part map as a function of frequency and parameter at value $E_F = 100$ meV, (c) the graphene conductivity real part map as a function of frequency and Fermi energy at value $u = 0.75 V_F$.

For the permittivity of graphene, we can write $\epsilon_g = 1 + i4\pi\sigma_g/\omega l_g$, since high-frequency conductivity and permittivity are related to each other by Maxwell’s equations. This means that the imaginary part of the permittivity of graphene $Im\epsilon_g = 4i\pi Re\sigma_g/\omega l_g$ at $Re\sigma_g < 0$ may turn out to be negative, which indicates the possibility of implementing amplification with a graphene monolayer in the specified range. Graphene layers can be in both unexcited and active states. In unexcited graphene, the Fermi energy E_F (chemical potential) is at the Dirac point and is equal to zero. In this case, the valence band is completely filled, the conduction band is completely free, and there is no band gap. It is possible to shift the chemical potential into the conduction band or valence band by applying a voltage of different polarity to a graphene sheet, and thereby change the surface conductivity of the graphene. A planar magnetic field applied in the plane of monolayers does not affect the electronic subsystem of graphene due to its 2D geometry.

3. Amplitude Characteristics of the Photonic Cell

Consider the transformation of transmission spectra with changes in the Fermi energy and magnetic field to identify the spectral features that arise when linearly polarized radiation passes through a PC. We assume that the incident wave falls on the PC normally to the plane of its layers and propagates along the symmetry axis of the structure. In this case, the inclination angle ψ_0 of the polarization plane, measured from the OX axis, can vary from 0 to 90° . For numerical analysis, we select the geometric parameters of the cell: the thickness of each of the side layers of the magnetic semiconductor is assumed to be equal to $L_1 = \lambda_0/4\sqrt{|\epsilon_\perp|} = 57 \mu\text{m}$, the thickness of the graphene monolayer is assumed to be $L_2 = 0.335$ nm, and the thickness of the dielectric (or air gap) is further considered to be a parameter. The wavelength $\lambda_0 = 749 \mu\text{m}$ corresponds to the operating frequency $f_0 = 0.4$ THz. For the air gap ($\epsilon_d = 1$), the optical and geometric thickness of the working cavity are the same.

The transfer matrix connecting the wave field at the input \mathbf{E}_0 and output $\mathbf{E}^{(t)}$ of the photonic cell has the form $G = (N_1 N_2) N_3 (N_2 N_1)$. Here N_j are the transfer matrices of individual layers, which in the plane wave approximation (valid for the above transverse dimensions of the layers) can be represented as follows:

$$N_j = \begin{pmatrix} \cos k_j L_j & i\sqrt{\varepsilon_j \mu_j} \sin k_j L_j \\ (i/\sqrt{\varepsilon_j \mu_j}) \sin k_j L_j & \cos k_j L_j \end{pmatrix}, \tag{5}$$

where $j = 1 - 3$, $k_j = k_0 \sqrt{\varepsilon_j \mu_j}$ are the propagation constants in the corresponding layers, $k_0 = \omega/c$, ω and c are the frequency and speed of the wave in vacuum. For dielectric layers $\varepsilon_j = \varepsilon_d$, $\mu_j = 1$, for graphene layers $\varepsilon_j = \varepsilon_{gr}$, $\mu_j = 1$, for semiconductor layers $\varepsilon_j = \varepsilon_{||}$, $\mu_{\perp} = 1$ in the case of a TE wave and $\varepsilon_j = \varepsilon_{\perp}$, $\mu_j = 1$ in the case of a TM wave.

The amplitude transmission and reflection coefficients for the entire structure are determined through the matrix elements of the transfer matrix G [23]:

$$t = \frac{2}{G_{11} + G_{12} + G_{21} + G_{22}}, \quad r = \frac{G_{11} + G_{12} - G_{21} - G_{22}}{G_{11} + G_{12} + G_{21} + G_{22}}. \tag{6}$$

If the polarization plane of the incident wave is oriented at an angle ψ_0 to the direction of the external magnetic field ($\mathbf{H}_0 \parallel Ox$), we represent the electric field of the wave incident on the photonic cell as follows:

$$\mathbf{E}_0 = \mathbf{e}_x E_0 \cos \psi_0 + \mathbf{e}_y E_0 \sin \psi_0. \tag{7}$$

At the exit from the photonic cell, the electric field is determined by the expression:

$$\mathbf{E}^{(t)} = E_0 (\mathbf{e}_x t^{TM} \cos \psi_0 + \mathbf{e}_y t^{TE} \sin \psi_0). \tag{8}$$

Taking into account the obtained expressions, the energy transmission and reflection coefficients can be presented as follows:

$$\begin{aligned} T(\psi_0) &= \frac{|E^{(t)}|^2}{E_0^2} = |t^{TM}|^2 \cos^2 \psi_0 + |t^{TE}|^2 \sin^2 \psi_0, \\ R(\psi_0) &= \frac{|E^{(r)}|^2}{E_0^2} = |r^{TM}|^2 \cos^2 \psi_0 + |r^{TE}|^2 \sin^2 \psi_0. \end{aligned} \tag{9}$$

When taking into account absorption (amplification) in the layers, the fraction of energy absorbed by the structure is determined by the quantity. If there is only absorption in the structure, if there is both absorption and amplification, the integral absorption coefficient can be either greater or less than zero.

Figure 4 for two photonic cells with a working cavity filled with a dielectric SiO₂ (a–c) and air (d–f), shows the frequency dependences of the transmission coefficients for incident waves with the orientation of the plane of polarization $\psi_0 = 0, 45^\circ, 90^\circ$ (green, blue, red curves), which become in the cell TM and TE waves of elliptical polarization, respectively. We chose silicon dioxide (SiO₂) as a dielectric, which is an optically isotropic material and has high optical transparency.

The optical thicknesses of the working cavity in both photonic cells are the same and equal $L'_3 = \lambda_0, \lambda_0/2, \lambda_0/4$, where $\lambda_0 = 749 \mu\text{m}$ corresponds to the operating frequency $f_0 = 0.4 \text{ THz}$, values $E_F = 0, H_0 = 0$. For dielectric SiO₂ in the terahertz range $\varepsilon_d = 5.07$ [34,35], the geometric thickness of the dielectric must be equal to $L_3^{(d)} = L_3^{(air)} / \sqrt{\varepsilon_d}$ so that the optical thicknesses of the dielectric and the air gap are equal. The optical anisotropy of a PC is determined by the presence of magnetically active layers CdCr₂Se₄ with a magnetization orientation directed along the OX axis (as in the applied magnetic field). It can be seen that significant changes occur in the spectrum with changes in the optical thickness of the dielectric (air gap). First of all, with decreasing L'_3 , the number of spectral peaks in the frequency range under consideration also decreases. With $L'_3 = \lambda_0/4$, a band gap appears

in the spectrum, similar to the well-developed photonic band gap in structures with a large number of periods. At $L'_3 = \lambda_0, \lambda_0/2$, a defect mode is observed at the center of the band gap (at frequency $f = 0.4$ THz), which is absent at thickness $L'_3 = \lambda_0/4$. Thus, at $L'_3 = \lambda_0$, an additional defect mode is also observed, which is split off from the right edge of the band gap. The indicated transformation of the spectrum is associated with a change in the phase relationships of the reflected waves in the photonic cell.

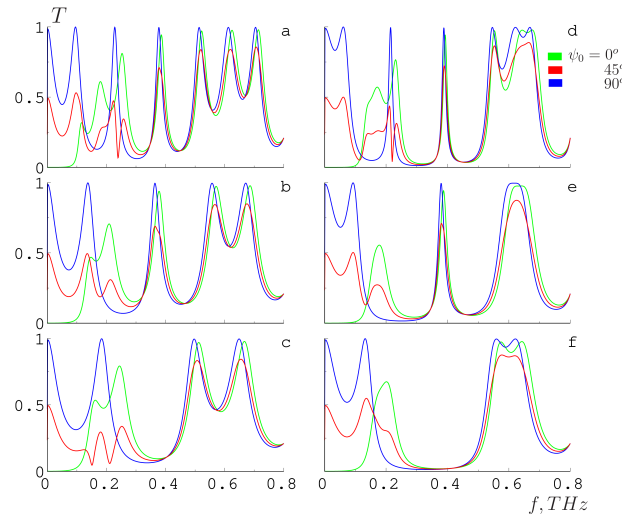


Figure 4. Frequency transmission spectra for a photonic cell with an optical thickness of the working cavity $L'_3 = \lambda_0, \lambda_0/2, \lambda_0/4$ filled with a dielectric (a–c) and air (d–f), at angles $\psi_0 = 0, 45^\circ, 90^\circ$ (green, red, blue curves) and $E_F, H_0 = 0$.

The nature of the given spectra also indicates that the strongest magneto-optical interaction with the structure is experienced by waves with the orientation of the polarization plane at the entrance to the photonic cell $\psi_0 = 0$, the weakest for waves with $\psi_0 = 90^\circ$. This is due to the fact that the first of these waves inside a photonic cell is a TM wave, the second is a TE wave. The most noticeable changes associated with the presence of graphene layers occur for waves with $\psi_0 = 45^\circ$ in the low-frequency region of the spectrum.

The spectrum of radiation passing through a photonic cell can be effectively controlled not only by the thickness of the air gap, but also by changing the energy state of graphene (i.e., its Fermi energy). Fermi energy control of graphene is based on its dependence on the external electric field strength E_s , which is given by [20,32] :

$$E_s = \frac{e}{\pi\hbar^2 V_F^2 \epsilon_b} \int_0^\infty \epsilon [f(\epsilon) - f(\epsilon + 2E_F)] d\epsilon, \tag{10}$$

where $f(\epsilon) = [\exp[(\epsilon - E_F)/k_B T] + 1]^{-1}$ is the Fermi-Dirac distribution, ϵ is the energy of the electron, $V_F = 3\gamma_0 b/2\hbar$ is the Fermi speed, where $\gamma_0 = 2.7$ eV, b is the distance between neighboring atoms in the graphene structure, ϵ_b is the dielectric constant of the substrate.

Figure 5 shows the dependence of the Fermi energy of graphene on the external constant electric field strength for $b = 0.142$ nm and the permittivity $\epsilon_b = 1, 5.07, 17.8$ of the substrate, respectively, for vacuum, SiO₂ and CdCr₂Se₄ (blue, red, green curves). It can be seen that with an increase in the external static field E_s applied to the graphene layer, the value of the Fermi energy increases the faster, the greater the permittivity of the substrate ϵ_b . In further numerical analysis, we assumed to use as a substrate for graphene SiO₂ (green curve).

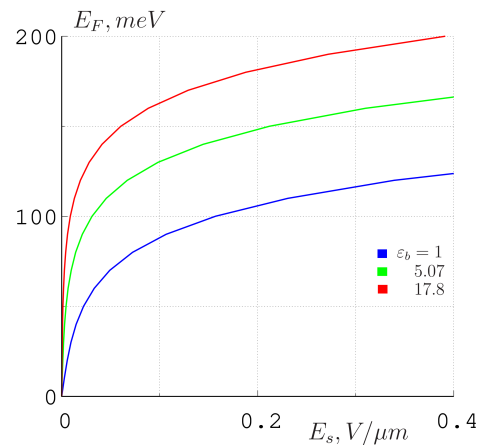


Figure 5. Dependence of the Fermi energy of graphene on the external electric field strength at $\epsilon_b = 1; 5.07; 17.8$ (blue, green, red curves).

Figure 6 shows the frequency dependence of the transmission and reflection coefficients at the angles of polarization plane orientation of the incident wave $\psi_0 = 0, 45^\circ, 90^\circ$ (green, red, blue curves), which were obtained for a photonic cell with $L'_3 = \lambda_0/2$, $E_F = (50, 100, 200)$ meV and $H_0 = (0, 2.5, 10)$ kOe.

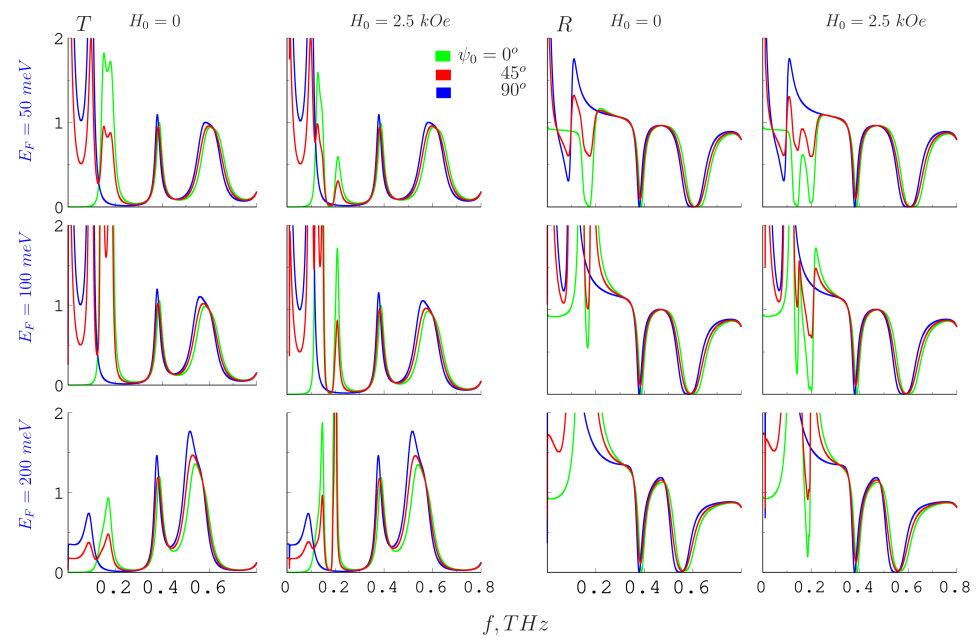


Figure 6. The frequency dependences of transmission coefficients at $\psi_0 = 0, 45^\circ, 90^\circ$ (green, red, blue curves), $E_F = (50, 100, 200)$ meV and $H_0 = (2.5, 10)$ kOe.

It can be seen that the transformation of the spectrum occurs with increasing Fermi energy, which is expressed primarily in the appearance of amplification in the low-frequency region. In this region, the transmission coefficient, as well as the reflection coefficient, become significantly greater than unity. The amplification region shifts from the region of low to the region of higher frequencies with increasing Fermi energy, and the magnitude of the amplification decreases, which is consistent with the dependence $\sigma'_g(E_F, f)$. In this case, a significant deformation of the band gap also occurs, associated with a shift of the low-frequency edge of the amplification to the region of higher frequencies. A slight increase in the amplitude of the defect mode, which also becomes greater than unity, is observed in the center of the band gap. It is characteristic that at $E_F = 200$ meV the transmission coefficients

in the low-frequency region do not exceed unity, while the defect mode and the value of T at the right edge of the band gap become significantly greater than unity. The reflectance spectra in the low-frequency region also experience significant changes depending on the magnitude of the magnetic field. In the high-frequency region, the spectrum changes $R(f)$ are insignificant. As the magnetic field increases, the most significant transformation is experienced by the spectra for waves with $\psi_0 = 0$, which become TM modes inside the photonic cell.

Figure 7 shows a map of the transmission coefficient when a linearly polarized wave is incident on a PC for three orientations of the polarization plane $\psi_0 = 0, 45^\circ, 90^\circ$. The thickness of the air gap of the cell is taken equal to $L'_3 = \lambda_0/2$. These maps determine the dependence of the coefficient T on frequency and Fermi energy at external magnetic field values $H_0 = (0, 2.5, 5, 10)$ kOe. For a clearer image of the amplification regions, we selected the low-frequency part of the spectrum and the transmission coefficient scale was limited to the value $T = 5$. Representing the transmission spectrum with tone diagrams makes it possible to convey the continuous dependence of the coefficient T on two parameters at once: frequency and Fermi energy. In particular, for the given values of ψ_0 and H_0 the regions of the parameters f and E_F are visible, where the amplification of the radiation propagating in the photonic cell is most effectively manifested.

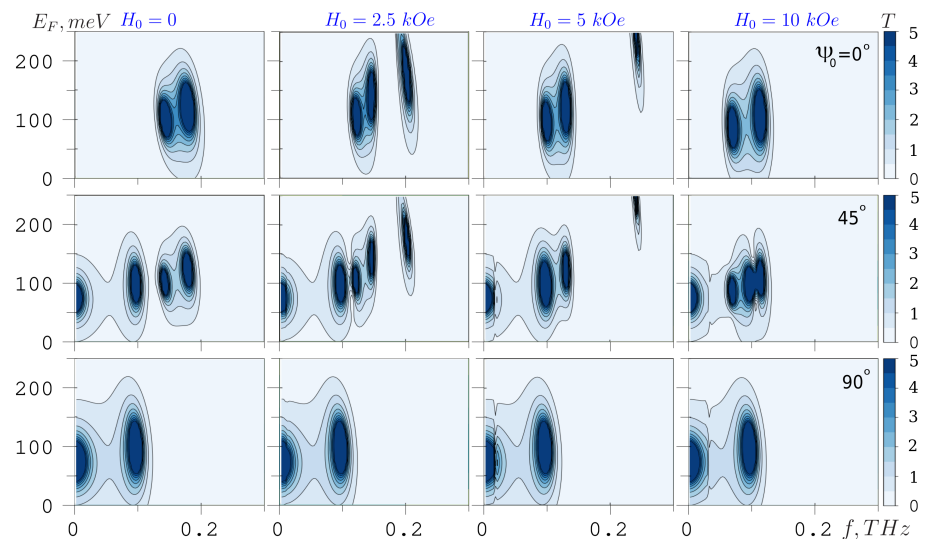


Figure 7. Transmission coefficient map as a function of frequency and Fermi energy, $\psi_0 = 0, 45^\circ, 90^\circ$, $L'_3 = \lambda_0/2$, $H_0 = (0, 2.5, 5, 10)$ kOe.

For example, one of the amplification regions for almost all values of H_0 has clear shapes for the parameters $\psi_0 = 45^\circ$, $f = 0.1$ THz and $E_F \approx 50 \div 110$ meV. For an angle of $\psi_0 = 45^\circ$, the amplification regions are the geometric sum of the amplification regions for waves with polarization angles $\psi_0 = 0^\circ$ and $\psi_0 = 90^\circ$, which is expressed in an increase in the number of amplification regions.

4. Polarization Characteristics of a Photonic Cell

To determine the polarization properties of a PC, we will assume that the plane of polarization of the incident wave is at an angle ψ_0 to the direction of the magnetizing field ($\mathbf{H}_0 \parallel OX$) and is determined by the direction of the electric vector of the wave in the plane xy . In the geometry under consideration, the eigenwaves for the photonic cell under study are waves of the TE and TM type with wave field components (H_x, E_y, H_z) and (E_x, H_y, E_z) , respectively. At the exit from the photonic cell, the components of the wave electric field are determined, according to Equation (8), by the following expressions:

$$E_x^{(t)} = A_{0x}t^{TM}, \quad E_y^{(t)} = A_{0y}t^{TE}, \tag{11}$$

where the corresponding amplitudes are: $A_{0x} = E_0 \cos \psi_0$, $A_{0y} = E_0 \sin \psi_0$. To describe the polarization state of a wave passing through a photonic cell, we introduce a complex polarization variable [36,37]:

$$\chi = \frac{|E_y^{(t)}|}{|E_x^{(t)}|} e^{i(\delta_y - \delta_x)} = \frac{A_{0y}}{A_{0x}} \frac{|t^{TE}|}{|t^{TM}|} e^{i(\delta^{TE} - \delta^{TM})}, \quad (12)$$

where $\delta^{TE} - \delta^{TM}$ is the phase mismatch of eigenwaves when passing through a photonic cell. The main polarization characteristics of the wave are the angle of inclination ψ of the major axis of the ellipse to the OX axis (azimuth of the polarization ellipse) and ellipticity \mathcal{E} , which is equal to the ratio of the semi-axes of the polarization ellipse and is determined by the ellipticity angle θ [36,37]:

$$\psi = \frac{1}{2} \arctan \frac{2\text{Re}\chi}{1 - |\chi|^2}, \quad \theta = -\frac{1}{2} \arcsin \frac{2\text{Im}\chi}{1 + |\chi|^2}, \quad \mathcal{E} = \tan \theta. \quad (13)$$

Since the transmission coefficients of TE and TM waves depend on the parameters that control the state of the structure, the polarization of the wave transmitted through the photonic cell can be controlled by changing the control parameters.

Figure 8a,b shows polarization ellipses corresponding to the magnetic field values $H_0 = (0, 2.5, 5, 10)$ kOe (red, green, blue, black lines) and: polarization angles of the incident wave ($\psi_0 = 0, 30^\circ, 60^\circ, 90^\circ$), Fermi energy $E_F = 110$ meV, frequency $f = 0.103$ THz (Figure 8a); polarization angle $\psi_0 = 45^\circ$ and different values of frequency and Fermi energy (indicated in Figure 8b).

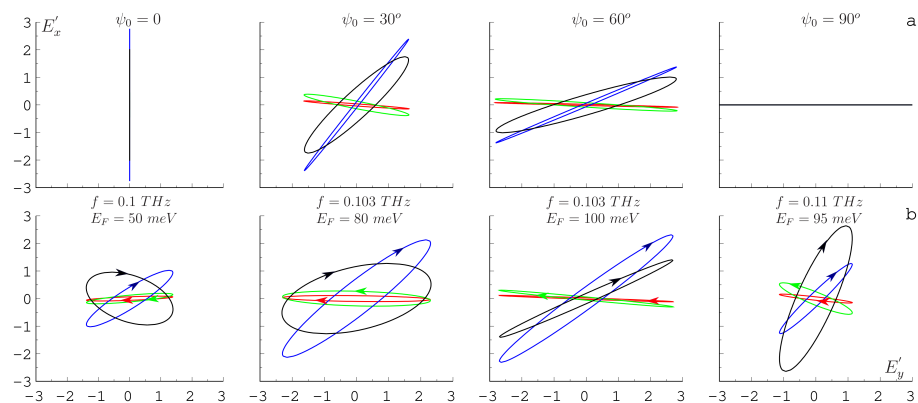


Figure 8. Polarization ellipses for field values $H_0 = (0, 2.5, 5, 10)$ kOe (red, green, blue and black lines) and $\psi_0 = 0, 30^\circ, 60^\circ, 90^\circ$, $E_F = 110$ meV, $f = 0.103$ THz (a); at $\psi_0 = 45^\circ$ and various values of frequency and Fermi energy, which are indicated in figures (b).

It can be seen that at angles $\psi_0 = 0$ and $\psi_0 = 90^\circ$ the polarization at the exit from the photonic cell does not change, i.e., the transmitted wave remains linearly polarized with the same orientation of the polarization plane. With increasing angle ψ_0 , the polarization of the transmitted wave becomes elliptical with ellipticity parameters depending on frequency, Fermi energy, external magnetic field and angle ψ_0 . The semimajor axis of the transmitted wave ellipse is greater than unity, since the selected frequency and Fermi energy value fall into the amplification region.

The polarization of the wave passing through the photonic cell can also be controlled at a fixed ψ_0 by changing other parameters, for example, the Fermi energy. Figure 8b shows the polarization ellipses of the transmitted wave at $\psi_0 = 45^\circ$ and various values of frequency and Fermi energy, which are indicated in the figures. The arrows in the figures indicate the direction in which the polarization ellipse is traversed as the wave propagates. Blue and black ellipses at the indicated frequencies correspond to left-handed polarized

waves (the electric field vector rotates clockwise), red and green ellipses correspond to right-handed polarized waves (the electric field vector rotates counterclockwise).

Figure 9 shows contour plots that determine the dependence of ellipticity as a function of frequency and Fermi energy for two values of the thickness of the air gap between the graphene layers $L'_3 = \lambda_0/2, \lambda_0/4$. Constant values of the magnetic field H_0 are marked in the figure, as well as lines of equal ellipticity levels. It can be seen that with an increase in the magnetic field, the transmitted right-handed polarized radiation changes to left-handed polarized; centers are also visible in which the ellipticity reaches maximum values $\mathcal{E} = \pm 1$, which corresponds to the degeneration of the ellipse into a circle with the corresponding direction of traversal of the electric field vector.

From a comparison of the given contour plots it follows that the position of the areas with the maximum and minimum ellipticity values, as well as changes in the direction of rotation of the electric vector, significantly depends on the thickness of the air gap L'_3 .

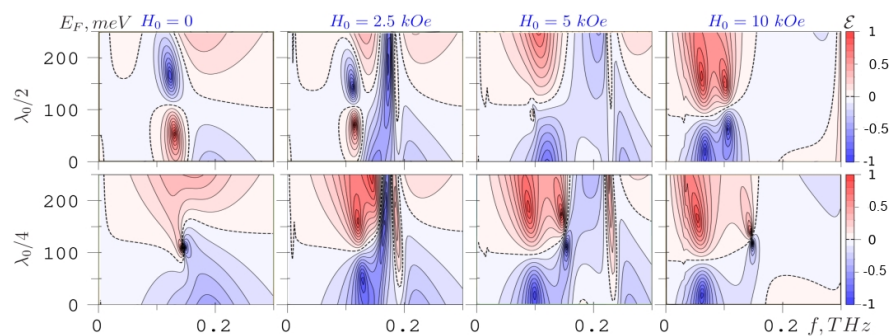


Figure 9. Ellipticity map as a function of frequency and Fermi energy for the thickness of the air gap between graphene layers $L'_3 = \lambda_0/2, \lambda_0/4$.

Thus, by changing the thickness of the air gap, it is also possible to control not only the parameters of the polarization ellipse, but also the rotation direction of the electric vector, i.e., type of transmitted wave.

5. Discussion

The study of layered periodic structures, which are used as functional elements, plays an important role in the development of current areas of science and technology. Therefore, close attention has been paid to the analysis of dispersion properties, reflectivity and transmission capacity of planar photonic crystal structures consisting of a large number of periods and various materials (passive and active) for many years. In this work, we study the optical properties of a photonic cell, which is a structure with a minimum number of periods, which makes it possible to implement a photonic band gap in its transmission spectrum and control its configuration and parameters using external electric and magnetic fields. For these purposes, the work considers one of the possible resonator-type photonic cells, consisting of two pairs of “magnetic semiconductor-graphene” layers and a dielectric layer between them.

The use of graphene in the structure is associated with the possibility of implementing amplification in the terahertz range, which can be achieved through several mechanisms. Thus, graphene with an inverted population of charge carriers, which can arise in graphene due to optical, injection or diffusion pumping, can act as an active medium for amplifiers and generators of THz radiation. However, for the near THz range it is promising to use graphene with charge carrier drift created by passing a high-density current through graphene without destroying it, due to technical and fundamental difficulties in creating inversion. Thus, to achieve a drift velocity $u = 0.8 V_F$, it is necessary to create an electric field with a strength of $15 \text{ V}/\mu\text{m}$, while the current density in graphene is $173 \text{ A}/\text{cm}$ at a Fermi energy of 200 meV [32].

The influence of a magnetic field on the properties of a magnetic semiconductor is associated with the resonant dependence of the components of its permittivity and permeability on the magnetic field strength, which is included in the expressions for the cyclotron frequency and the ferromagnetic resonance frequency. Free electrons of a magnetic semiconductor begin to rotate around the magnetic field lines at a frequency close to the cyclotron resonance frequency, which interferes with the propagation of an electromagnetic wave inside the material. Spin oscillations will be excited in a magnetic semiconductor, which also impedes the penetration of an electromagnetic wave into the medium at frequencies close to the ferromagnetic resonance frequency (microwave range), which should lead to a decrease in the transmission coefficient.

A magnetic field applied in the plane of graphene layers, due to their transverse monoatomicity, does not affect the dynamics of electrons. Since the radius of the cyclotron orbit $R_c = mv/eB$, even at $B \sim 10$ T, is much greater than the thickness of graphene, in this case the magneto-optical effect in graphene is strongly suppressed, which does not lead to the influence of the magnetic field on the transmission (reflection) coefficients.

Thus, the transformation of the spectra can be achieved both by changing the Fermi energy of graphene and its conductivity under the influence of an external electric field, and by changing the permittivity and permeability of the magnetic semiconductor layers when exposed to an external magnetic field.

6. Conclusions

In this paper, the frequency dependencies of the transmission coefficient of linearly polarized radiation passed through a symmetric photonic cell are obtained. The cell is represented by two layers of magnetic semiconductor, each of which is coated with a monolayer of graphene, and separated by a layer of air or a dielectric medium. Graphene is in an active state, in which the drift of charge carriers is achieved due to current pumping. Effective control of transmission spectra is achieved by changing parameters such as the Fermi energy, external magnetic field, air gap thickness and orientation of the polarization plane of the incident wave on the photonic cell. In particular, a change in the Fermi energy of graphene leads to a significant increase in radiation in the low-frequency terahertz region of the spectrum, where the transmission coefficient can reach values significantly exceeding unity.

Contour plots of the dependence of the transmission coefficient on frequency, Fermi energy and external magnetic field are presented, which determine the shape of the amplification regions of transmitted radiation (low-frequency and high-frequency boundaries) and the distribution of the transmission coefficient over this region. The ellipticity's map versus on the Fermi energy and external magnetic field at a fixed frequency demonstrates the possibility of controlling the polarization of transmitted radiation. Thus, it is possible to change the transmitted radiation from right-polarized to left-polarized with increasing magnetic field. Contour plots allow you to identify the centers of parameter areas with maximum ellipticity values ($\mathcal{E} = \pm 1$). It is possible to control the ellipticity and direction of rotation of the electric vector by changing the thickness of the air gap in the photonic cell.

Such a photonic cell can be used as an active medium in a photonic resonator structure or as a functional element of an optical system as a polarizer with controlled parameters of the polarization ellipse with amplification of the transmission coefficient or the type of transmitted wave.

Author Contributions: Conceptualization, D.I.S.; methodology, S.V.E. and P.A.I.; software, S.V.E.; formal analysis, S.V.E. and P.A.I.; funding, P.A.I.; investigation, S.V.E. and D.I.S.; resources, D.I.S.; data curation, S.V.E.; writing—original draft preparation, P.A.I. and D.I.S.; writing—review and editing, S.V.E.; supervision, D.I.S.; project administration, D.I.S. All authors have read and agreed to the published version of the manuscript.

Funding: The work is supported by the Russian Science Foundation (project 23-79-30017) and Ministry of Education and Science of the Russian Federation (project 075-15-2021-581).

Data Availability Statement: Data are contained within the article.

Conflicts of Interest: The authors declare no conflict of interest. The funders had no role in the design of the study; in the collection, analyses, or interpretation of data; in the writing of the manuscript, or in the decision to publish the results.

Abbreviations

The following abbreviations are used in this manuscript:

PC	photonic cell
BMs	Bragg mirrors

References

1. Heebner, J.; Grover, R.; Ibrahim, T. *Optical Microresonator Theory, Fabrication, and Applications*; Springer: Berlin/Heidelberg, Germany, 2008; p. 268.
2. Hodgson, N.; Weber, H. *Optical Resonators: Fundamentals, Advanced Concepts, Applications*; Springer Science & Business Media: Berlin/Heidelberg, Germany, 2005; p. 795.
3. Matsko, A.B. *Practical Applications of Microresonators in Optics and Photonics*; CRC Press: Boca Raton, FL, USA, 2018; p. 586.
4. Chremmos, I.; Schwelb, O.; Uzunoglu, N. *Photonic Microresonator Research and Applications*; Springer: Berlin/Heidelberg, Germany, 2010; p. 530.
5. Averkov, Y.O.; Yakovenko, V.; Yampol'Skii, V.; Nori, F. Terahertz transverse-electric- and transverse-magnetic-polarized waves localized on graphene in photonic crystals. *Phys. Rev. B* **2014**, *90*, 045415. [[CrossRef](#)]
6. Mogni, E.; Pellegrini, G.; Gil-Rostra, J.; Yubero, F.; Simone, G.; Fossati, S.; Dostálek, J.; Martínez Vázquez, R.; Osellame, R.; Celebrano, M.; et al. One-Dimensional Photonic Crystal for Surface Mode Polarization Control. *Adv. Opt. Mater.* **2022**, *10*, 2200759. [[CrossRef](#)]
7. Charik, H.; Bouras, M.; Bennacer, H. High-sensitive thermal sensor based on a 1D photonic crystal microcavity with nematic liquid crystal. *Prog. Electromagn. Res. M* **2021**, *100*, 187–195. [[CrossRef](#)]
8. Qi, L.; Liu, C. Complex band structures of 1D anisotropic graphene photonic crystal. *Photonics Res.* **2017**, *5*, 543–551. [[CrossRef](#)]
9. Bayindir, M.; Kural, C.; Ozbay, E. Coupled optical microcavities in one-dimensional photonic bandgap structures. *J. Opt. A Pure Appl. Opt.* **2001**, *3*, S184. [[CrossRef](#)]
10. Lei, F.; Ward, J.M.; Romagnoli, P.; Chormaic, S.N. Polarization-controlled cavity input-output relations. *Phys. Rev. Lett.* **2020**, *124*, 103902. [[CrossRef](#)] [[PubMed](#)]
11. Mahmoodzadeh, H.; Rezaei, B. Tunable Bragg defect mode in one-dimensional photonic crystal containing a graphene-embedded defect layer. *Appl. Opt.* **2018**, *57*, 2172–2176. [[CrossRef](#)]
12. Mohebbi, M. Refractive index sensing of gases based on a one-dimensional photonic crystal nanocavity. *J. Sens. Sens. Syst.* **2015**, *4*, 209–215. [[CrossRef](#)]
13. AL-Zahrani, H.A.M. Simulation and design of photonic crystal with nonlinear components. *Sciences* **2018**, *8*, 690–704.
14. Arkhipkin, V.; Gunyakov, V.; Myslivets, S.; Gerasimov, V.; Zyryanov, V.Y.; Vetrov, S.Y.; Shabanov, V. One-dimensional photonic crystals with a planar oriented nematic layer: Temperature and angular dependence of the spectra of defect modes. *J. Exp. Theor. Phys.* **2008**, *106*, 388–398. [[CrossRef](#)]
15. Morozov, S.V.; Novoselov, K.S.; Geim, A.K. Electron transport in graphene. *Physics-Uspokhi* **2008**, *51*, 744–748. [[CrossRef](#)]
16. Falkovsky, L.A. Optical properties of graphene and IV–VI semiconductors. *Physics-Uspokhi* **2008**, *51*, 887. [[CrossRef](#)]
17. Aleshkin, V.Y.; Dubinov, A.A.; Ryzhii, V. Terahertz laser based on optically pumped graphene: Model and feasibility of realization. *Jetp Lett.* **2009**, *89*, 63–67. [[CrossRef](#)]
18. Sheehy, D.E.; Schmalian, J. Optical transparency of graphene as determined by the fine-structure constant. *Phys. Rev. B* **2009**, *80*, 193411. [[CrossRef](#)]
19. Rut'kov, E.V.; Lavrovskaya, N.P.; Sheshenya, E.S.; Gall, N.R. Optical transparency of graphene layers grown on metal surfaces. *Semiconductors* **2017**, *51*, 492–497. [[CrossRef](#)]
20. Morozov, M.Y.; Moiseenko, I.; Popov, V. Giant amplification of terahertz plasmons in a double-layer graphene. *J. Phys. Condens. Matter* **2018**, *30*, 08LT02. [[CrossRef](#)] [[PubMed](#)]
21. Evseev, D.A.; Eliseeva, S.V.; Sementsov, D.I.; Shutyi, A.M. A Surface Plasmon–Polariton in a Symmetric Dielectric Waveguide with Active Graphene Plates. *Photonics* **2022**, *9*, 587. [[CrossRef](#)]
22. Eliseeva, S.; Sementsov, D. Spectra of a Bragg Microcavity with an Active Graphene Medium. *Bull. Russ. Acad. Sci. Phys.* **2022**, *86*, 1144–1150. [[CrossRef](#)]
23. Mercado-Zúñiga, C.; Gallegos-García, G.; Trejo-Valdez, M.; Martínez-Rivas, A.; Vargas-García, J.R.; Torres-Torres, C. All-optical encryption by a heterodyne Kerr gate in multilayer reduced graphene oxide decorated with Pt nanoparticles. *Opt. Mater.* **2021**, *119*, 111324. [[CrossRef](#)]
24. Niu, F.; Zhang, H.; Yuan, J.; Xiao, L.; Jia, S.; Wang, L. Photonic graphene with reconfigurable geometric structures in coherent atomic ensembles. *Front. Phys.* **2023**, *18*, 52304. [[CrossRef](#)]

25. Shadrivov, I.V.; Kapitanova, P.V.; Maslovski, S.I.; Kivshar, Y.S. Metamaterials controlled with light. *Phys. Rev. Lett.* **2012**, *109*, 083902. [[CrossRef](#)] [[PubMed](#)]
26. Kuzmin, D.A.; Bychkov, I.V.; Shavrov, V.G. Electromagnetic waves reflection, transmission and absorption by graphene–magnetic semiconductor–graphene sandwich-structure in magnetic field: Faraday geometry. *Photonics Nanostruct. Fundam. Appl.* **2014**, *12*, 473–481. [[CrossRef](#)]
27. Dietl, T. A ten-year perspective on dilute magnetic semiconductors and oxides. *Nat. Mater.* **2010**, *9*, 965–974. [[CrossRef](#)] [[PubMed](#)]
28. Bass, F.G.; Bulgakov, A.A.; Teterov, A.P. *High-Frequency Properties of Semiconductors with Superlattices*; Moscow Izdatel Nauka: Moscow, Russia, 1989; p. 288.
29. Gurevich, A.G.; Melkov, G.A. *Magnetization Oscillations and Waves*; CRC Press: Boca Raton, FL, USA, 2020; p. 464.
30. Svintsov, D. Emission of plasmons by drifting Dirac electrons: A hallmark of hydrodynamic transport. *Phys. Rev. B* **2019**, *100*, 195428. [[CrossRef](#)]
31. Moiseenko, I.; Popov, V.; Fateev, D. Terahertz plasmon amplification in a double-layer graphene structure with direct electric current in hydrodynamic regime. *Phys. Rev. B* **2021**, *103*, 195430. [[CrossRef](#)]
32. Moiseenko, I.M.; Popov, V.V.; Fateev, D.V. Amplification of terahertz electromagnetic waves in a structure with two graphene layers under a direct electric current flow: A hydrodynamic approximation. *Semiconductors* **2021**, *55*, S30–S34. [[CrossRef](#)]
33. Fedorova, I.V.; Eliseeva, S.V.; Sementsov, D.I. Transmission and Reflection Spectra of a Bragg Microcavity Filled with a Periodic Graphene-Containing Structure. *Appl. Sci.* **2023**, *13*, 7559. [[CrossRef](#)]
34. Hung, H.C.; Wu, C.J.; Chang, S.J. Terahertz temperature-dependent defect mode in a semiconductor-dielectric photonic crystal. *J. Appl. Phys.* **2011**, *110*, 093110. [[CrossRef](#)]
35. El-Naggar, S.A. Tunable terahertz omnidirectional photonic gap in one dimensional graphene-based photonic crystals. *Opt. Quantum Electron.* **2015**, *47*, 1627–1636. [[CrossRef](#)]
36. Born, M.; Wolf, E. *Principles of Optics: Electromagnetic Theory of Propagation, Interference and Diffraction of Light*; Elsevier: Amsterdam, The Netherlands, 2013; p. 952.
37. Yariv, A.; Yeh, P. *Optical Waves in Crystals*; Wiley: New York, NY, USA, 1984; p. 604.

Disclaimer/Publisher’s Note: The statements, opinions and data contained in all publications are solely those of the individual author(s) and contributor(s) and not of MDPI and/or the editor(s). MDPI and/or the editor(s) disclaim responsibility for any injury to people or property resulting from any ideas, methods, instructions or products referred to in the content.